Chiral nanosurfaces for enhancement of local electromagnetic field

Lukas Ohnoutek[a,b,*], Ventsislav K. Valev[a,b]
[a]Centre for Photonics and Photonic Materials, University of Bath, Bath, BA2 7AY, U. K.;
[b]Centre for Nanoscience and Nanotechnology, University of Bath, Bath, BA2 7AY, U. K.

ABSTRACT

The ability of plasmonic nanosurfaces to produce strong electromagnetic fields in their vicinity upon illumination can be used to enhance effects, such as those originating from chirality (lack of mirror symmetry) of molecules. We numerically investigate chiral nanosurfaces composed of plasmonic nanobars with varying packing densities. We identify the optimum illumination conditions for maximal field enhancement. Under these illumination conditions, the optical chirality near the surface exceeds the optical chirality of the incident light by almost an order of magnitude in a large area (200 nm × 200 nm) near the surface. Our simulations prove the nanosurfaces to be promising candidates for enhancement of chiral-optical effects.

Keywords: chirality, optical chirality, nanosurface, field enhancement, plasmonics

1. INTRODUCTION

Chiral molecules, i.e. molecules lacking mirror symmetry, are widely used in pharmaceuticals. While their effects on the human body can vary significantly depending on the handedness of the molecules,[1,2] determination of enantiomeric excess (excess of one chiral version of the molecule) in solutions is often based on measuring chiral-optical (chiroptical) effects, which are typically weak.[3]

Nanostructured surfaces (nanosurfaces) made of plasmonic metals have been investigated as means of enhancing these weak chiroptical effects.[4,5] The enhancement can arise from the nanosurface concentrating incident light into tiny areas with large electromagnetic fields. Thus, the molecules located in these areas experience stronger levels of illumination. Furthermore, if the nanosurface is chiral, its near field is chiral as well. Whereas the chirality in the nanostructures is quantified by the geometric chirality parameter,[6] the chirality of electromagnetic fields is quantified by optical chirality C.[7,8] A chiral nanosurface can be designed so that the optical chirality near its surface is larger than the optical chirality of circularly polarized light in free space, which then leads to enhancement of chiroptical effects.

Various designs of plasmonic nanosurfaces have been investigated, e.g. arrays of G-,[9–11] S-,[12] U-,[13,14] C-,[15] Z-,[16] and L-shapes,[17,18] that have been studied, for instance, with second harmonic generation - an interface sensitive technique.[19,20] Various numerical methods have been proposed in order to tune the electromagnetic fields in metal nanostructures.[21,22]

In this work, we numerically study the electromagnetic near fields of nanosurfaces composed of Au bars arranged in a chiral pattern. Previously, similar structures with varying widths of the bars were investigated.[23] Here, we identify the optimum packing density to achieve maximal enhancement of the chiroptical response.

2. SAMPLES

The nanosurfaces we investigate in this work are shown in Figure 1. As can be seen in Figure 1(a), the nanosurfaces are made up of bars, which are 200 nm wide and 200 nm apart from each other. The arrangement of the bars leads to creation of chiral centers on the surface. There are two different types of chiral centers, as illustrated in the figure. These two centers have different sizes and opposite chirality. Changing the length L of the bars changes the contribution of the two types of chiral centers and determines their density of packing. In this work, the length was varied from 400 nm up to 1000 nm in 200-nm increments.

The profile of the simulated samples is illustrated in Figure 1(b). The bars are made up of Au on top of a thin Cr layer. The substrate is oxidized Si. This profile was chosen in a way so that samples with identical design can later be fabricated.

*L.Ohnoutek@bath.ac.uk

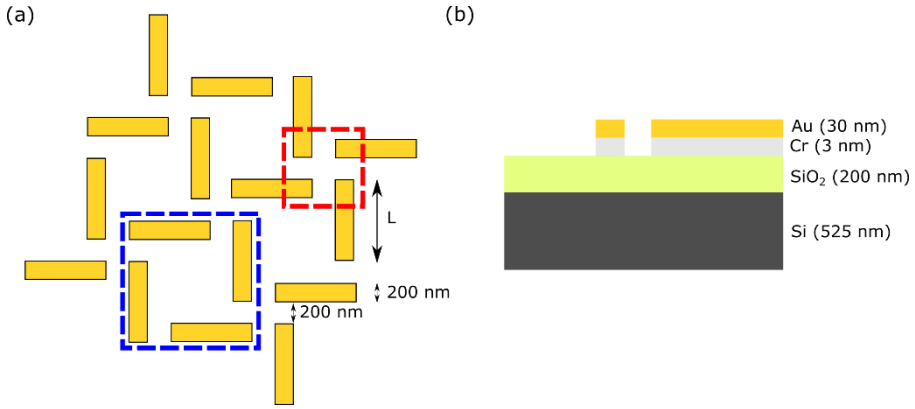

Figure 1. Chiral nanosurfaces with variable packing density. (a) Illustration of the arrangement of the plasmonic nanobars with varying length L on the surface of the sample. Two types of chiral centers are indicated with the dashed red and blue squares. (b) The cross-section of the simulated structures.

3. METHODOLOGY

Finite-difference time-domain (FDTD) simulations[24–26] in Lumerical FDTD were carried out to obtain the electromagnetic fields in the vicinity of the nanosurface. The optical constants of Si, SiO_2, and Cr had been measured by Palik.[27] The optical properties of Au had been measured by Johnson and Christy.[28]

The size of the simulation region in the plane of the nanosurface varied with the length of the Au bars. The simulation region was chosen in such a way so that periodic boundary conditions could be applied. The dimensions were 2.6 μm × 2.6 μm, 2 μm × 2 μm, 5.8 μm × 5.8 μm, and 4 μm × 4 μm for the nanosurfaces with 400-nm, 600-nm, 800-nm, and 1000-nm bars, respectively. In the direction perpendicular to the surface, the simulation region spanned 1.2 μm. A perfectly matched layer (PMA)[29] was used on both simulation region boundaries in this direction.

Two plane wave light sources were located 0.6 μm above the top of the SiO_2 layer. The wavelength range of the sources was set to be from 450 nm to 1100 nm. To achieve illumination with circularly polarized light, the polarization angle and the phase were different for the two sources. Here, we denote the illuminating light as left circularly polarized (LCP) when the polarization angle and phase of the first source were both set to 0 degrees and the polarization angle and phase of the second source were both set to 90 degrees. For right circularly polarized light, the phase of the second source was changed to -90 degrees.

Electromagnetic fields were recorded 1 nm above the surface of the sample for wavelengths from 450 nm to 1100 nm in steps of 50 nm.

4. RESULTS

Upon illumination, coherent oscillations of electrons, called surface plasmons, can be induced on the edges of the bars forming the nanosurface. The nature of the excited plasmonic modes depends on the wavelength and polarization state of the incident light, as well as the length of the bars. The oscillations of charges induce electromagnetic fields in their vicinity. These near fields lead to electromagnetic coupling between the bars on the nanosurface. The superposition of the induced fields can create areas with high electromagnetic fields near the surface.

We would like to obtain strong electromagnetic fields over a large region near the surface. Thus, we want to identify the illumination conditions (wavelength and direction of circular polarization), which lead to maximum fields in the dashed red square shown in Figure 1(a).

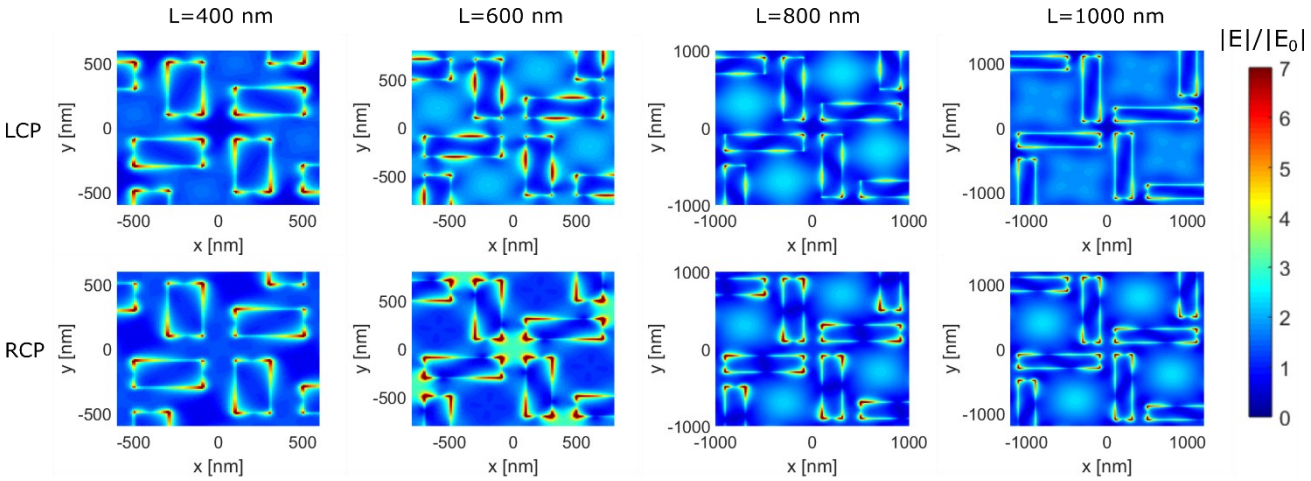

Figure 2. Color maps visualizing the electric field 1 nm above the surface of the samples upon illumination with 900-nm light. The amplitude of the electric field is normalized to the electric field amplitude of the incident light E_0. The four columns correspond to the four different Au bar lengths L, which are indicated at the top of the columns. The top panels show results for illumination with left circularly polarized (LCP), the bottom ones for right circularly polarized (RCP) light.

Figure 2 shows the electric field amplitudes normalized to the amplitude of the incident light E_0 slightly above the sample's surface for illumination at 900 nm. The incident light is either left circularly polarized (LCP) or right circularly polarized (RCP). The normalized amplitudes of the electric field are plotted as color maps.

For all lengths of the Au bars, there are areas with large field enhancement. Some of these arise from the lightning rod effect – the accumulation of electrons in sharp corners due to increased density of electromagnetic field lines. The areas of large enhancement on the edges of the Au bars are due to plasmonic modes excited by the incident light. As discussed above, the nature of the excited modes varies with the length of the Au bars. This variation than leads to changes in the near field close to the edges of the bars, which can be seen in Figure 2. The calculated near fields also change significantly with the polarization of the incident light, as expected.

The maximum field is induced in the smaller of the chiral centers when the nanosurface with 600-nm bars is illuminated with RCP light. In this case, an electric field with a relative amplitude of approximately 3 is induced over the region. Molecules located in this large region would thus experience stronger illumination levels.

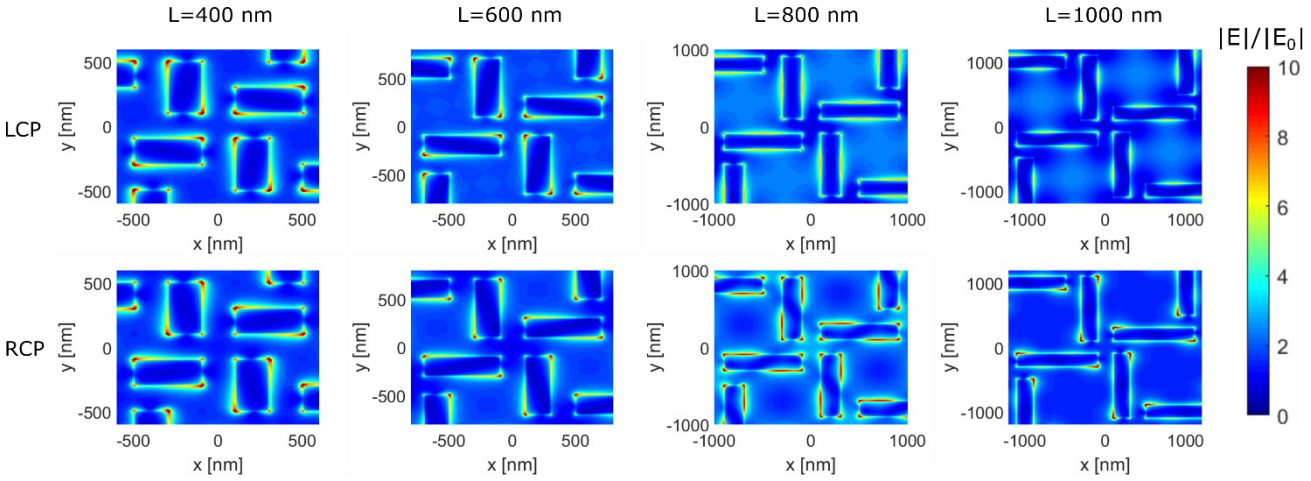

Figure 3. Color maps visualizing the electric field 1 nm above the surface of the samples upon illumination with 1100-nm light. The amplitude of the electric field is normalized to the electric field amplitude of the incident light E_0. The four columns correspond to the four different Au bar lengths L, which are indicated at the top of the columns. The top panels show results for illumination with left circularly polarized (LCP), the bottom ones for right circularly polarized (RCP) light.

As discussed at the beginning of this section, the near field of the nanosurface changes with the wavelength of the incident light as well. The near fields calculated for illumination with 1100-nm shown in Figure 3 are indeed different to the ones in Figure 2. In both cases, there are areas of large electric fields along the edges of the Au bars, which arise from pronounced plasmonic resonances. However, at this wavelength, enhancement in the center of the plotted region can be seen for the nanosurface with 800-nm bars. The relative field amplitude in the central region is approximately 2.8.

Interactions of light with molecules placed on the nanosurface will be enhanced by the strong near field. Further enhancement of chiroptical effects can be achieved by the near field being superchiral. i.e. its optical chirality being larger than optical chirality of circularly polarized light.

Optical chirality C can be calculated from[30]

$$C = -\frac{\varepsilon_0 \omega}{2} \mathrm{Im}[\boldsymbol{E}^* \cdot \boldsymbol{B}], \tag{1}$$

where ε_0 is the vacuum permittivity, ω the angular frequency of the light, $\boldsymbol{E}$ the complex electric field amplitude, and $\boldsymbol{B}$ the complex magnetic field amplitude.

The optical chirality of circularly polarized light is equal to[7]

$$C_{CPL} = \pm \frac{\varepsilon_0 \omega}{2c} |\boldsymbol{E}|^2, \tag{2}$$

where c is the speed of light.

We can use equation (1) to calculate the optical chirality for the configurations with large field enhancement discussed above. To provide insight into how the optical chirality near the nanosurface compares to the optical chirality in free space, the calculated optical chirality is normalized to the optical chirality of circularly polarized light obtained from equation (2). In equation (2), we use $|\boldsymbol{E}| = 1$, which is the amplitude of the incident light in our simulations. The resultant relative optical chirality is presented in Figure 4. In both (a) and (b), the optical chirality is enhanced almost by an order of magnitude in a large region close to the surface of the sample, compared to the optical chirality of circularly polarized light in free space.

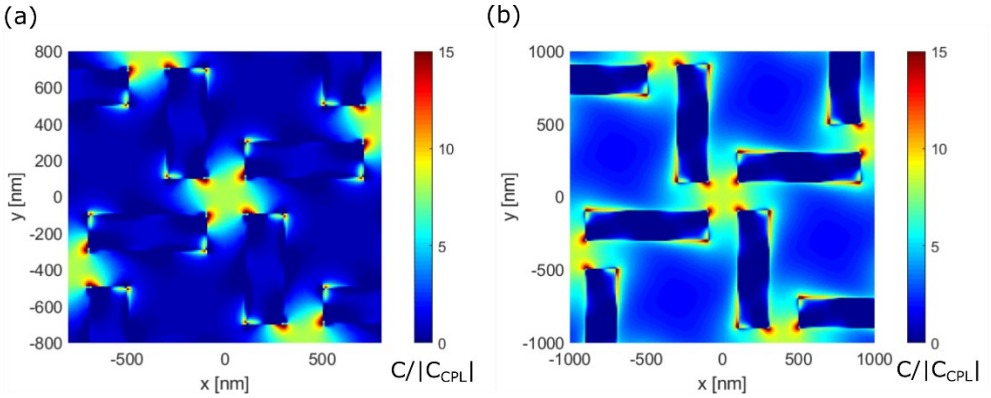

Figure 4. Optical chirality is enhanced in the chiral centers on the nanosurfaces. The calculated optical chirality is normalized to the modulus of optical chirality of the incident circularly polarized light $|C_{CPL}|$. Optical chirality is plotted as a color map for (a) a nanosurface made up of 600-nm Au bars illuminated with right circularly polarized 900-nm light, (b) a nanosurface made up of 800-nm Au bars illuminated with right circularly polarized 1100-nm light.

The combination of large electromagnetic fields and enhanced optical chirality in a large region near the surface makes these nanosurfaces extremely promising for sensitive measurements of chiral molecules.

5. CONCLUSIONS

In summary, we presented numerical calculations of near fields of plasmonic nanosurfaces with varying dimensions. The results prove the nanosurfaces to be promising candidates for applications benefiting from strong electromagnetic field concentration, such as nonlinear optical effects, surface-enhanced Raman spectroscopy (SERS) and molecular sensing. We have identified the optimal illumination conditions for different nanosurface designs. The optical chirality near the nanosurfaces is higher than in free space in a large region, which evidences the potential for enhancement of chiroptical

responses of molecules. Next, we will prepare samples with these dimensions and will demonstrate their enhanced chiroptical properties.

ACKNOWLEDGEMENTS

Data created during this research is openly available from the University of Bath Research Data Archive at https://doi.org/10.15125/BATH-00992.[31]

V.K.V. acknowledges support from the Royal Society through the University Research Fellowships and the Royal Society grants PEF1\170015 and RGF\EA\180228, as well as the STFC grant ST/R005842/1. L.O. and V.K.V. acknowledge funding and support from the Engineering and Physical Sciences Research Council (EPSRC) Centre for Doctoral Training in Condensed Matter Physics (CDT-CMP), Grant No. EP/L015544/1 and EP/T001046/1.

REFERENCES

[1] Franks, M. E., Macpherson, G. R. and Figg, W. D., "Thalidomide," Lancet **363**(9423), 1802–1811 (2004).
[2] H. Brooks, W., C. Guida, W. and G. Daniel, K., "The Significance of Chirality in Drug Design and Development," Curr. Top. Med. Chem. **11**(7), 760–770 (2011).
[3] Mun, J., Kim, M., Yang, Y., Badloe, T., Ni, J., Chen, Y., Qiu, C.-W. and Rho, J., "Electromagnetic chirality: from fundamentals to nontraditional chiroptical phenomena," Light Sci. Appl. **9**(1), 139 (2020).
[4] Kuppe, C., Zheng, X., Williams, C., Murphy, A. W. A., Collins, J. T., Gordeev, S. N., Vandenbosch, G. A. E. and Valev, V. K., "Measuring optical activity in the far-field from a racemic nanomaterial: diffraction spectroscopy from plasmonic nanogratings," Nanoscale Horizons **4**(5), 1056–1062 (2019).
[5] Gansel, J. K., Wegener, M., Burger, S. and Linden, S., "Gold helix photonic metamaterials: A numerical parameter study," Opt. Express **18**(2), 1059 (2010).
[6] Pendry, J. B., "A Chiral Route to Negative Refraction," Science **306**(5700), 1353–1355 (2004).
[7] Tang, Y. and Cohen, A. E., "Optical Chirality and Its Interaction with Matter," Phys. Rev. Lett. **104**(16), 163901 (2010).
[8] Tang, Y. and Cohen, A. E., "Enhanced Enantioselectivity in Excitation of Chiral Molecules by Superchiral Light," Science **332**(6027), 333–336 (2011).
[9] Valev, V. K., Smisdom, N., Silhanek, A. V., De Clercq, B., Gillijns, W., Ameloot, M., Moshchalkov, V. V. and Verbiest, T., "Plasmonic Ratchet Wheels: Switching Circular Dichroism by Arranging Chiral Nanostructures," Nano Lett. **9**(11), 3945–3948 (2009).
[10] Mamonov, E. A., Murzina, T. V., Kolmychek, I. A., Maydykovsky, A. I., Valev, V. K., Silhanek, A. V., Verbiest, T., Moshchalkov, V. V. and Aktsipetrov, O. A., "Chirality in nonlinear-optical response of planar G-shaped nanostructures," Opt. Express **20**(8), 8518 (2012).
[11] Mamonov, E. A., Kolmychek, I. A., Vandendriessche, S., Hojeij, M., Ekinci, Y., Valev, V. K., Verbiest, T. and Murzina, T. V., "Anisotropy versus circular dichroism in second harmonic generation from fourfold symmetric arrays of G-shaped nanostructures," Phys. Rev. B **89**(12), 121113 (2014).
[12] Narushima, T., Hashiyada, S. and Okamoto, H., "Nanoscopic Study on Developing Optical Activity with Increasing Chirality for Two-Dimensional Metal Nanostructures," ACS Photonics **1**(8), 732–738 (2014).
[13] Decker, M., Zhao, R., Soukoulis, C. M., Linden, S. and Wegener, M., "Twisted split-ring-resonator photonic metamaterial with huge optical activity," Opt. Lett. **35**(10), 1593 (2010).
[14] Liu, N., Liu, H., Zhu, S. and Giessen, H., "Stereometamaterials," Nat. Photonics **3**(3), 157–162 (2009).
[15] Belardini, A., Larciprete, M. C., Centini, M., Fazio, E., Sibilia, C., Chiappe, D., Martella, C., Toma, A., Giordano, M. and Buatier de Mongeot, F., "Circular Dichroism in the Optical Second-Harmonic Emission of Curved Gold Metal Nanowires," Phys. Rev. Lett. **107**(25), 257401 (2011).
[16] Su, H., Guo, Y., Gao, W., Ma, J., Zhong, Y., Tam, W. Y., Chan, C. T. and Wong, K. S., "Multipolar Effects in the Optical Active Second Harmonic Generation from Sawtooth Chiral Metamaterials," Sci. Rep. **6**(1), 22061 (2016).
[17] Valev, V. K., Baumberg, J. J., De Clercq, B., Braz, N., Zheng, X., Osley, E. J., Vandendriessche, S., Hojeij, M., Blejean, C., Mertens, J., Biris, C. G., Volskiy, V., Ameloot, M., Ekinci, Y., Vandenbosch, G. A. E.,

Warburton, P. A., Moshchalkov, V. V, Panoiu, N. C. and Verbiest, T., "Nonlinear Superchiral Meta-Surfaces: Tuning Chirality and Disentangling Non-Reciprocity at the Nanoscale," Adv. Mater. **26**(24), 4074–4081 (2014).

[18] Canfield, B. K., Kujala, S., Laiho, K., Jefimovs, K., Turunen, J. and Kauranen, M., "Chirality arising from small defects in gold nanoparticle arrays," Opt. Express **14**(2), 950 (2006).

[19] Valev, V. K., Kirilyuk, A., Dalla Longa, F., Kohlhepp, J. T., Koopmans, B. and Rasing, T., "Observation of periodic oscillations in magnetization-induced second harmonic generation at the Mn/Co interface," Phys. Rev. B **75**(1), 012401 (2007).

[20] Vincent, B., Loo, R., Vandervorst, W., Delmotte, J., Douhard, B., Valev, V. K., Vanbel, M., Verbiest, T., Rip, J., Brijs, B., Conard, T., Claypool, C., Takeuchi, S., Zaima, S., Mitard, J., De Jaeger, B., Dekoster, J. and Caymax, M., "Si passivation for Ge pMOSFETs: Impact of Si cap growth conditions," Solid. State. Electron. **60**(1), 116–121 (2011).

[21] Zheng, X., Valev, V. K., Verellen, N., Jeyaram, Y., Silhanek, A. V., Metlushko, V., Ameloot, M., Vandenbosch, G. A. E. and Moshchalkov, V. V., "Volumetric Method of Moments and Conceptual Multilevel Building Blocks for Nanotopologies," IEEE Photonics J. **4**(1), 267–282 (2012).

[22] Xuezhi Zheng, Volskiy, V., Valev, V. K., Vandenbosch, G. A. E. and Moshchalkov, V. V., "Line Position and Quality Factor of Plasmonic Resonances Beyond the Quasi-Static Limit: A Full-Wave Eigenmode Analysis Route," IEEE J. Sel. Top. Quantum Electron. **19**(3), 4600908–4600908 (2013).

[23] Collins, J. T., Zheng, X., Braz, N. V. S., Slenders, E., Zu, S., Vandenbosch, G. A. E., Moshchalkov, V. V., Fang, Z., Ameloot, M., Warburton, P. A. and Valev, V. K., "Enantiomorphing Chiral Plasmonic Nanostructures: A Counterintuitive Sign Reversal of the Nonlinear Circular Dichroism," Adv. Opt. Mater. **6**(14), 1800153 (2018).

[24] Taflove, A. and Hagness, S. C., [Computational electrodynamics: the finite-difference time-domain method, 3rd ed.], Boston, Mass.; London: Artech House (2005).

[25] Teixeira, F. L., "Time-Domain Finite-Difference and Finite-Element Methods for Maxwell Equations in Complex Media," IEEE Trans. Antennas Propag. **56**(8), 2150–2166 (2008).

[26] Montgomery, J. M., Lee, T.-W. and Gray, S. K., "Theory and modeling of light interactions with metallic nanostructures," J. Phys. Condens. Matter **20**(32), 323201 (2008).

[27] Palik, E. D., [Handbook of Optical Constants of Solids], Academic Press, Orlando; London (1985).

[28] Johnson, P. B. and Christy, R. W., "Optical Constants of the Noble Metals," Phys. Rev. B **6**(12), 4370–4379 (1972).

[29] Berenger, J.-P., "Perfectly matched layer for the FDTD solution of wave-structure interaction problems," IEEE Trans. Antennas Propag. **44**(1), 110–117 (1996).

[30] Collins, J. T., Kuppe, C., Hooper, D. C., Sibilia, C., Centini, M. and Valev, V. K., "Chirality and Chiroptical Effects in Metal Nanostructures: Fundamentals and Current Trends," Adv. Opt. Mater. **5**(16), 1700182 (2017).

[31] Ohnoutek, L., Valev, V., "Dataset for "Chiral nanosurfaces for enhancement of local electromagnetic field"," Bath: University of Bath Research Data Archive (2021). https://doi.org/10.15125/BATH-00992